



# Quantifying the Near-term Response of the Ocean CO<sub>2</sub> Sink to Emissions Mitigation

5 Amanda R. Fay<sup>1</sup>, Dustin Carroll<sup>2,3</sup>, Galen A. McKinley<sup>1</sup>, Nicole S. Lovenduski<sup>4</sup>, Dimitris Menemenlis<sup>2</sup>,  
Hong Zhang<sup>3</sup>

<sup>1</sup>Columbia University and Lamont-Doherty Earth Observatory, Palisades, NY, USA

<sup>2</sup>Moss Landing Marine Laboratories, San José State University, Moss Landing, CA, USA

<sup>3</sup>Jet Propulsion Laboratory, California Institute of Technology, Pasadena, USA

10 <sup>4</sup>University of Colorado, Boulder, CO, USA

*Correspondence to:* Amanda R. Fay (afay@ldeo.columbia.edu)

**Abstract.** The ocean plays a critical role in sequestering carbon, yet how the air-sea carbon sink will respond to rapid reductions in atmospheric carbon dioxide (CO<sub>2</sub>) concentrations remains a key uncertainty for climate mitigation and carbon accounting. In this study, we utilize the ECCO-Darwin ocean biogeochemistry model to simulate the ocean's response to a range of near-term CO<sub>2</sub> mitigation scenarios. Our results demonstrate an immediate but spatially heterogeneous weakening of the ocean carbon sink following reduced atmospheric forcing. Global air-sea carbon uptake decreases substantially within the first several years of mitigation, with the magnitude of the reduction scaling with the strength of the mitigation scenario. We find that the mitigation signal is primarily confined to the upper-500 m, reflecting dominant decadal-scale ventilation pathways. The most pronounced reductions in uptake occur in subtropical thermocline regions, western boundary currents, and the subpolar North Atlantic — regions characterized by intense ventilation and rapid air-sea equilibration. These findings align with recent CMIP-based long-term projections and observation-based inversions, confirming that the areas currently dominating anthropogenic carbon uptake are also the most sensitive to atmospheric forcing changes. Our results suggest that observational efforts to track mitigation impacts should be prioritized in these high-latitude and boundary current systems, where signals emerge earliest and most strongly. Ultimately, this study underscores the rapid sensitivity of the ocean carbon sink to changes in atmospheric forcing and highlights the necessity of sustained, strategically-placed observations to detect and attribute changes in the global carbon budget under future climate strategies.

## Introduction

30 The oceans absorb a substantial fraction of anthropogenic emissions of carbon dioxide (CO<sub>2</sub>), acting as a vital buffer for atmospheric CO<sub>2</sub> rise and thereby moderating the impact of climate change (Gruber et al., 2019, 2023, Friedlingstein et al., 2025). However, the capacity, efficiency, and changing patterns of the future ocean carbon sink remain highly uncertain across different emission scenarios. Consequently, it is unclear how future mitigation pathways will affect the sink's long-term trajectory and durability.



35

Past studies that consider the global ocean response to climate mitigation have relied on fully-coupled Earth System Models (ESMs), with dynamic feedbacks between model components. Katavouta & Williams (2021) examined basin-scale contributions to the carbon-concentration and carbon-climate feedbacks across various ESMs who carried out experiments under the 6th Coupled Model Intercomparison Project (CMIP6). Their work demonstrates that ocean basins differ markedly in how ventilation, seawater buffer chemistry, and marine biology drive future CO<sub>2</sub> uptake patterns. While ESMs provide a detailed representation of physical, chemical, and biological processes, they are computationally demanding and typically explore a limited set of scenarios (Flato et al., 2013).

At the same time, several studies underscore the regional and mechanistic complexity of the ocean carbon sink under both warming and mitigation. For example, Williams et al. (2024) highlight the pronounced role of the Southern Ocean in global carbon uptake and its asymmetries under changing atmospheric forcing. They find that the North Atlantic exhibits a larger reduction in carbon uptake than the Southern Ocean in future Shared Socioeconomic Pathway (SSP) scenarios using the CMIP6 suite of models (O'Neill et al., 2016, Riahi et al., 2017). Furthermore, Lee et al. (2025) demonstrate that under strong warming, an “uptake hole” may emerge in the subpolar North Atlantic due to shifts in convection and ventilation. These studies emphasize how regional ocean dynamics, transport, and vertical redistribution of dissolved inorganic carbon (DIC) are as important as surface forcing (i.e., air-sea gas exchange) when considering the long-term impact of changing CO<sub>2</sub> emissions and ocean carbon sequestration. Specifically, the Southern Ocean has emerged as a critical region for anthropogenic carbon uptake, often accounting for ~40 % of the global-ocean sink. Terhaar et al. (2021) used an emergent constraint approach to access the Southern Ocean’s cumulative uptake during 1850–2100, with uptake of 158±6 Pg C under SSP1-2.6 and 279±14 Pg C under SSP5-8.5. They found that sea surface salinity in the frontal zone between the Subtropical and Polar Front, which is primarily regulated by the freshwater cycle and circulation, is a key process regulating the ventilation and associated deep sequestration of anthropogenic carbon in the Southern Ocean.

Additionally, previous studies have revealed important mechanistic transitions that occur during emission mitigation scenarios. Ridge & McKinley (2021) showed that under high-emission scenarios, the decline in ocean uptake efficiency is dominated by buffer-capacity decline (a chemical limitation), whereas under a strong mitigation target, this decline is dominated by reduced vertical transport of anthropogenic carbon (a physical limitation) as the gradient between surface and interior carbon is reduced. This difference in the driving limitation of continued ocean carbon uptake under very different future climate scenarios illuminates the need for continued ocean monitoring and process studies to identify and better predict the trajectory of the ocean sink in the 21st century and beyond.

Despite the growing body of model- and process-based research, there remain important gaps in understanding how rapid, strong mitigation might reshape the magnitude, timing, and regional-scale footprint of ocean carbon uptake. In this study, we



adopt an assimilation-based modelling framework, using the Estimating the Circulation and Climate of the Ocean-Darwin  
70 (ECCO-Darwin) ocean biogeochemistry model. We employ the ECCO-Darwin framework to isolate the oceanic carbon-  
cycle response to prescribed atmospheric CO<sub>2</sub> mitigation under physically consistent and observationally-constrained ocean  
physics and circulation. This approach avoids confounding carbon-climate feedbacks (Schimel and Carroll, 2024, Carroll et  
al., 2025) from atmosphere-sea-ice coupling while enabling a clear mechanistic interpretation of ventilation and carbon  
storage pathways on decadal timescales. ECCO-Darwin offers a unique balance between realism and interpretability by  
75 combining a globally optimized, observation-constrained hydrography, sea ice, and circulation with full marine carbon and  
ecosystem cycling. This makes it particularly well-suited for diagnosing regional and vertical mechanisms governing early  
mitigation responses, which are more difficult to isolate in fully- coupled ESMs.

## 2. Methods

80

### 2.1 Experimental Design and Atmospheric CO<sub>2</sub> Forcing

We conducted a set of forward simulations using the v05 ECCO-Darwin ocean biogeochemistry model; a detailed  
description of the v05 ECCO-Darwin model set-up, observational constraints, and optimization methodology is presented in  
Carroll et al. (2020). Our Baseline simulation represents a best-possible hindcast of the ocean's physical, sea ice, and  
85 biogeochemical state from 1985–2021. The model is forced with observed atmospheric xCO<sub>2</sub> from the National Oceanic and  
Atmospheric Administration Marine Boundary Layer product (NOAA MBL, Lan et al., 2024) and ECCO LLC 270 physics  
(Zhang et al., 2018). Model set-up and results from the Baseline simulation are discussed in more detail in Fay et al. (2024).

In this study, we generate and analyze output from three scenarios using different atmospheric forcing for years 2000–2021:

90

1. **Baseline:** forced with observed atmospheric CO<sub>2</sub> concentrations from NOAA MBL.
2. **SSP1 Mitigation:** forced with a prescribed atmospheric CO<sub>2</sub> trajectory consistent with projections based on  
SSP1-1.9, representing a strong mitigation.
3. **SSP2 Mitigation:** forced with a trajectory consistent with SSP1-2.6, representing moderate mitigation.

95

Using atmospheric xCO<sub>2</sub> projections for SSP1-1.9 and SSP1-2.6 mitigation pathways, provided by the Model for the  
Assessment of Greenhouse Gas Induced Climate Change (MAGICC) project (Meinshausen et al., 2020), we adjust the  
atmospheric carbon mixing ratio values back in time to impose changes beginning in January 2000 (Figure 1, Figure S1).  
This experimental setup provides an estimate of how ocean carbon uptake would evolve over the recent observation period if  
emission mitigation had started in 2000. This novel use of a contemporary model and time period, with projected mitigation  
100 scenarios applied backward in time, provides unique insight into how the ocean carbon sink responds to mitigation signals  
within decadal timescales.



Experiment Name	Atmospheric Forcing
Baseline	Observed NOAA MBL $x\text{CO}_2$
SSP1 Mitigation	SSP1-1.9 trajectory after year 2000
SSP2 Mitigation	SSP1-2.6 trajectory after year 2000

**Table 1.** List of model experiments and prescribed atmospheric forcing. NOAA = National Oceanic and Atmospheric Administration Marine Boundary Layer (MBL) Product.  $x\text{CO}_2$  is the column-averaged  $\text{CO}_2$  carbon dioxide in the atmosphere, represented in parts per million (Lan et al., 2024). Shared socio-economic pathway (SSP) trajectories were obtained from the MAGICC project (<https://live.magicc.org/>, Meinshausen et al. 2020).

In this model configuration, ECCO-Darwin model physics are derived from the solution of Fay et al. (2024) and have identical physical characteristics in the baseline and mitigation runs. This allows us to isolate the carbon-cycle response (i.e., air-sea  $\text{CO}_2$  flux, seawater  $p\text{CO}_2$ , DIC perturbation) to observed and mitigated atmospheric  $\text{CO}_2$  forcing without confounding changes in the physical and sea-ice ocean state. Each simulation uses identical physical and biogeochemical initial conditions. Differences among scenarios and the baseline therefore reflect the dynamic response of ocean circulation and carbonate chemistry to changes in atmospheric  $\text{CO}_2$  concentration alone. Furthermore, we compute three-dimensional DIC budget terms for each simulation, as done in Carroll et al. (2022), to provide mechanistic insight into the drivers of DIC space-time variability.

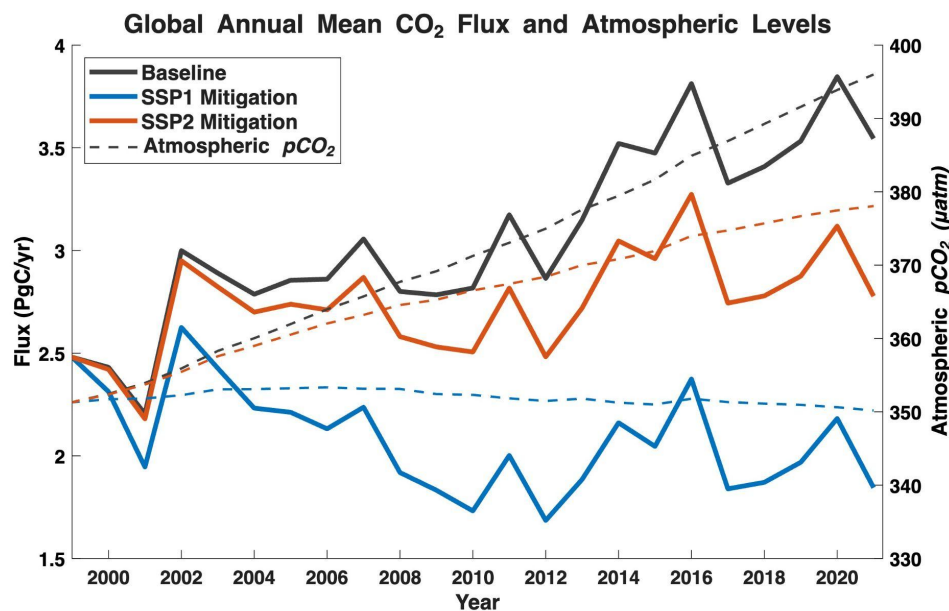


**Figure 1:** Annual-mean time series of air-sea CO<sub>2</sub> flux (solid lines) and atmospheric pCO<sub>2</sub> (dashed lines) for Baseline (black) and SSP mitigation simulations (SSP1: Blue, SSP2: Orange). Air-sea CO<sub>2</sub> flux is globally integrated, and surface atmosphere pCO<sub>2</sub> represents a global mean. Time series starts in year 2000, when SSP scenario forcing is applied. Positive flux represents ocean uptake (for the purpose of comparing with atmospheric values). Full time series available in Figure S1.

### 3. Results

This section presents the simulated response of the marine carbon cycle under two divergent mitigation trajectories — SSP1 and SSP2 — as compared to the ECCO-Darwin Baseline run (Table 1). While both scenarios are evaluated, the following analysis primarily focuses on SSP1, as its aggressive mitigation pathway provides a more pronounced signal for identifying the mechanisms of carbon flux and storage change. Throughout this section, results are generally interpreted as the difference (or delta) between the mitigation scenario and the baseline (i.e. Mitigation minus Baseline), with a focus on the resulting differences in air-sea exchange and interior inventory. We first examine global atmospheric forcing and flux responses before detailing the physical and chemical drivers of carbon distribution across interior, spatial, and basin-scale dimensions, culminating in a comprehensive DIC budget analysis.

#### 3.1 Atmospheric Forcing and Global Air-Sea CO<sub>2</sub> Flux Response

Simulated global air-sea CO<sub>2</sub> fluxes diverge immediately post mitigation, responding promptly to changes in atmospheric carbon levels (Figure 1). The three atmospheric CO<sub>2</sub> scenarios diverge immediately following the onset of mitigation in January 2000, with SSP1 Mitigation representing the most aggressive reduction and SSP2 being a more moderate pathway (Figure 1, Table 1). Reacting to the increasing atmospheric carbon levels in the Baseline simulation, ocean CO<sub>2</sub> uptake



continues to increase steadily through 2021. In contrast, the SSP1 simulation exhibits an immediate, marked reduction in uptake, while SSP2 Mitigation follows an intermediate trajectory between Baseline and SSP1 runs. For both mitigation  
140 scenarios, correlations between the detrended time series of global mean flux and atmospheric  $p\text{CO}_2$  levels for 2000–2021 show positive correlations of 0.48 at the 95% confidence level. The strength of global mean air-sea  $\text{CO}_2$  flux reduction due to mitigation is on the order of 48% and 22% for SSP1 and SSP2 Mitigation scenarios, respectively, by the end of the simulation (2021, Figure 1 and Figure S1).

145 Although air-sea  $\text{CO}_2$  flux and atmospheric  $\text{CO}_2$  forcing are not strictly proportional, global annual-mean  $\text{CO}_2$  uptake closely tracks the imposed atmospheric trend, with the magnitude of flux reduction scaling with the strength of mitigation (Figure 1). Considering the mean over the last six years of the simulation (2016–2021), the atmosphere experiences a 10% decrease in  $p\text{CO}_2$  between the Baseline and SSP1 Mitigation scenarios ( $351\mu\text{atm}$  vs  $390\mu\text{atm}$ ) and 4% decrease between Baseline and SSP2 ( $376\mu\text{atm}$  vs  $390\mu\text{atm}$ ). For the same time period, the decrease in air-sea flux is nearly  $1.6 \text{ PgC yr}^{-1}$  (SSP1–Baseline),  
150 equivalent to 45% of the Baseline flux estimate (Figure 1). For SSP2 Mitigation the difference is  $0.65 \text{ PgC yr}^{-1}$  (SSP2–Baseline), equivalent to 18% of the Baseline flux estimate (Figure 1). Decreasing the air-sea atmospheric  $p\text{CO}_2$  gradient through mitigation directly and rapidly alters the net ocean carbon flux.

### 3.2 Interior Carbon Response

155 Mitigation causes a marked decrease in the interior ocean DIC inventory (Figure 2). In SSP1, significant upper ocean  $\Delta\text{DIC}$  values (Mitigation minus Baseline) are evident within the first few years post mitigation, reaching as high as 1 Tmol difference in the surface ocean by 2005 (Figure 2a). This response is consistent with the rapid stabilization of atmospheric  $\text{CO}_2$  in SSP1 (Figure 1). The largest difference in DIC inventory occurs around 500 m depth at the end of the simulation, reaching as high as 7.5 Tmol more DIC in the Baseline run compared to the strong SSP1 mitigation scenario (Figure 2a).  
160 Under the more gradual SSP2 mitigation scenario, such pronounced differences in DIC are not apparent. The maximum difference in DIC inventory reaches only 2 Tmol by 2021, however, the spatial patterns remain consistent, with largest differences occurring around 400–500 m depth (Figure 2b). For both mitigation scenarios, DIC levels below 1500 m depth are indistinguishable from the Baseline run (not shown). Mitigation-driven changes remain confined to the upper ~1000 m of the water column over the 21-year simulation period. The global ocean time series of the upper ocean's  $\Delta\text{DIC}$  inventory also  
165 illustrate these patterns (Figure 2c). The volume-integrated upper ocean DIC inventory (0–500 m) increases steadily in the Baseline simulation but begins to diverge sharply in SSP1 mitigation, with a smaller but detectable divergence under SSP2 (Figure 2c).

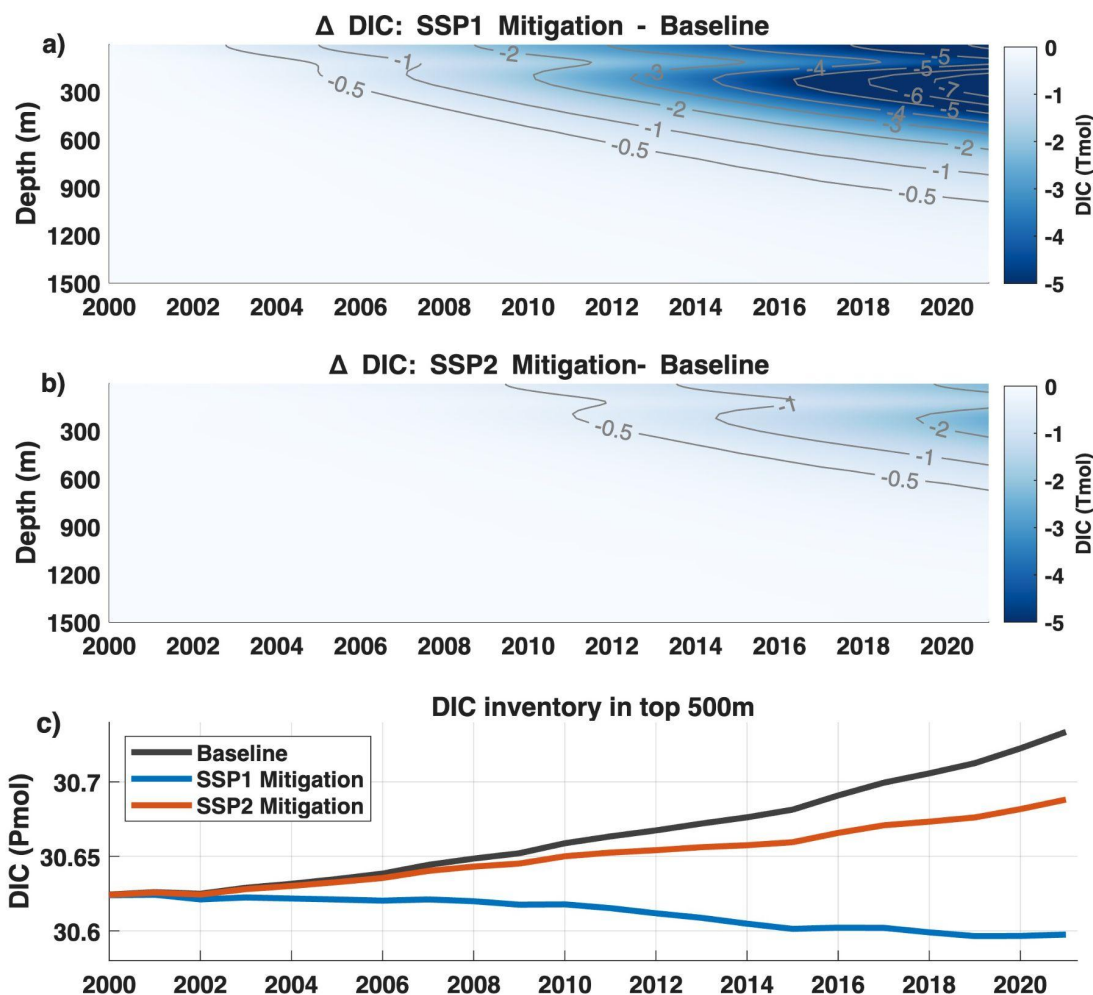


**Figure 2:** Globally-integrated  $\Delta$ DIC. Differences between Baseline and **a)** SSP1 and **b)** SSP2 for upper 1500 m. **c)** time series of DIC inventory in top 500 m of the upper ocean for Baseline (black) and SSP scenarios (SSP1 Mitigation: blue; SSP2 Mitigation: orange).

### 3.3 Spatial Patterns of Air–Sea CO<sub>2</sub> Flux Change

The Baseline simulation exhibits a large-scale pattern of air-sea CO<sub>2</sub> flux, with strong net CO<sub>2</sub> uptake in the mid-latitude Southern Ocean, the subpolar North Atlantic, and the western boundary current systems of the North Pacific and North Atlantic (Figure 3a). Similar patterns of uptake and efflux exist for SSP1 and SSP2 Mitigation simulations (Figure 3b,c), however, the strength of uptake is diminished in the mitigation simulations. Differences relative to the Baseline for the end



of the experiments (2016–2021 mean) reveal pronounced regional heterogeneity in the response to mitigation (Figure 3d,e). Both SSP1 and SSP2 Mitigation simulations show widespread reductions in ocean CO<sub>2</sub> uptake relative to Baseline, with the magnitude of change larger under SSP1 Mitigation but the patterns relatively unchanged (Figure 3d,e). The spatial structure of these differences indicates that mitigation does not uniformly weaken uptake across the global ocean, but instead produces concentrated responses in specific ocean regions characterized by distinct circulation dynamics.

The largest reductions in cumulative CO<sub>2</sub> uptake occur in the Southern and North Atlantic and Pacific Oceans, identifying these regions as primary hotspots of mitigation sensitivity. In the ECCO-Darwin experimental runs, the North Pacific Kuroshio region (NP STSS biome, Fay & McKinley 2014) exhibits a 17% decrease in flux between the Baseline and SSP1 Mitigation experiment by the final year of the simulation. A smaller reduction (8%) is produced by the SSP2 Mitigation experiment in 2021. For the North Atlantic boundary current region (NA STSS biome, Fay & McKinley 2014), the reduction in carbon uptake by the end of the simulation is even more pronounced: 24.5% for SSP1 Mitigation and 11% for SSP2 Mitigation. The pronounced reductions in air-sea CO<sub>2</sub> flux observed in these regions under both SSP1 and SSP2 Mitigation scenario forcings reflect their efficiency as conduits for anthropogenic carbon, as well as their sensitivity to changes in atmospheric CO<sub>2</sub> concentrations.

Another dynamic area which exhibits a strong response to mitigation is the Southern Ocean. Located within the core flow of the Antarctic Circumpolar Current (ACC), the Southern Ocean subpolar region (SO SPSS biome, Fay & McKinley 2014) reduction in carbon uptake by the end of the simulation is even more pronounced: 56% for SSP1 Mitigation and 24% for SSP2 Mitigation (Figure 3d,e). In contrast, large portions of the northern and southern subtropical gyres exhibit weaker deltas and thus slower adjustment to changes in atmospheric CO<sub>2</sub> over the mitigation experiment.

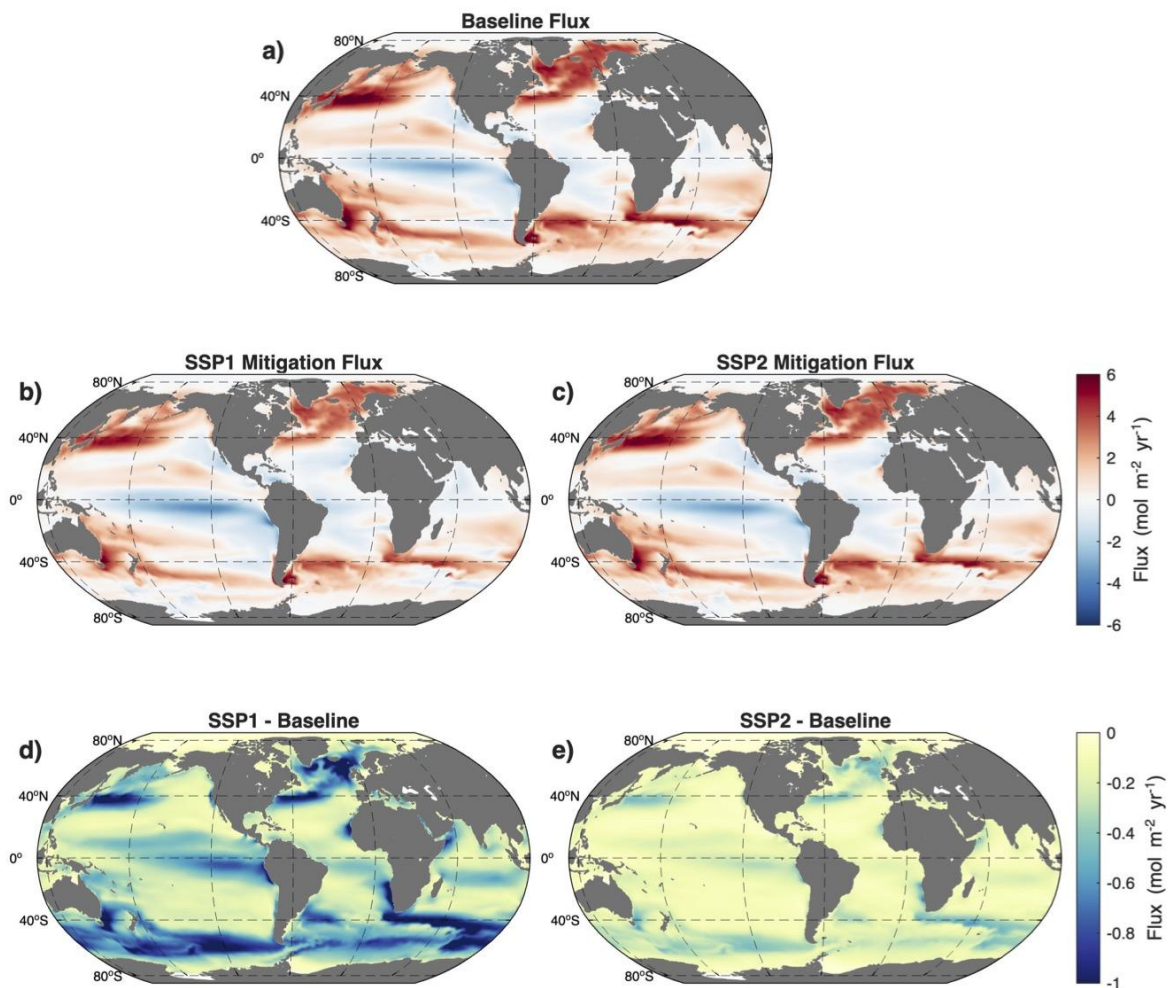


**Figure 3:** Mean air-sea CO<sub>2</sub> flux (mol m<sup>-2</sup> yr<sup>-1</sup>) over 2016–2021, for **a)** Baseline **b)** SSP1 Mitigation and **c)** SSP2 Mitigation, with differences from Baseline shown in **d)** SSP1 Mitigation minus Baseline and **e)** SSP2 Mitigation minus Baseline. In **a-c**, red colors represent ocean uptake and blue colors indicate regions of outgassing. In difference maps (**d,e**) blue areas indicate regions where there is less uptake (more outgassing) in the Mitigation experiments compared to the Baseline scenario. Neither mitigation scenario results in ocean areas with increased uptake as compared to the Baseline run.

### 210 3.4 Zonal and Basin-Scale Carbon Distribution

Zonally-averaged ΔDIC concentrations (Mitigation minus Baseline) reveal clear differences in the timing, depth penetration, and basin dependence of the mitigation signal (Figure 4).



In the Southern Ocean (latitudes  $<40^{\circ}\text{S}$  in Figure 4a,b), zonal-mean  $\Delta\text{DIC}$  values (SSP1 minus Baseline) exhibit a distinct  
215 structure; DIC differences appear quickly at depth and span a broad vertical range. By 2011, DIC differences extended below  
100-m depth across much of the basin. By 2021, mitigation-driven differences are distributed throughout the upper and mid-  
depth Southern Ocean, however, they remain constrained to the top 1000 m. This pattern suggests rapid vertical  
communication of changes in surface forcing, consistent with the vigorous mixing and overturning characteristics of the  
Southern Ocean. The largest differences are observed along the equatorial edge of the Southern Ocean, with differences in  
220 DIC of  $10\text{ mmol m}^{-3}$  reaching down to nearly 500 m. Figure 3d shows that the largest changes in surface air-sea flux are  
evident in the Southern Ocean, while Figure 4 demonstrates that the excess carbon absorbed in the Baseline simulation is  
quickly transported and mixed into the deeper ocean.

In the Atlantic Ocean (Figure 4, righthand side), DIC differences between SSP1 Mitigation and Baseline emerge rapidly  
225 following the onset of mitigation; negative values indicate greater DIC accumulation in the Baseline relative to SSP1  
Mitigation. Minimal differences are evident in the first year post-mitigation, and are confined to the surface and upper  
thermocline (Figure S2). By 2011,  $\Delta\text{DIC}$  values intensify and extend downward to depths of  $\sim 500\text{--}700\text{ m}$ , particularly in the  
mid latitudes of the Northern Hemisphere (Figure 4a). By the end of the simulation (2021, Figure 4b), the largest DIC  
differences span much of the upper 500 m, with pronounced signals along known ventilation pathways that connect surface  
230 waters to the ocean interior including the subpolar gyre and Labrador Sea in North Atlantic and along the ACC in the  
Southern hemisphere. In the latitudes of the subpolar North Atlantic, differences due to mitigation reach deeper into the  
ocean column and are evident at 1500 m. In the surface layers, the largest mitigation differences occur in 2021 in the  
subtropical latitudes ( $20\text{--}40^{\circ}\text{N}$ ). This indicates that the Baseline run contains much more DIC, yielding negative  $\Delta\text{DIC}$   
values (SSP Mitigation minus Baseline). Carbon absorbed in these subtropical areas is not transported to depth because the  
235 ocean is highly stratified, creating a physical barrier that limits mixing with deeper waters.

The temporal evolution of zonal  $\Delta\text{DIC}$  highlights a progressive deepening of the mitigation signal. In the Atlantic, the  
downward propagation of DIC mitigation differences under SSP1 is most evident between approximately  $40^{\circ}\text{N}$  and  $60^{\circ}\text{N}$ ,  
consistent with regions of active mode and intermediate water formation.  $\Delta\text{DIC}$  values in the Southern Hemisphere are  
240 weaker in magnitude at the surface in 2021 (Figure 4b) but extend deeper as the simulation progresses, indicating efficient  
vertical redistribution. The contrasting vertical structures between basins indicate that the response of interior carbon storage  
to mitigation is strongly modulated by distinct, regional circulation and ventilation regimes. Across all time periods,  
differences between SSP1 and SSP2 Mitigation follow a similar spatial structure, with larger  $\Delta\text{DIC}$  magnitudes under SSP1  
Mitigation reflecting the stronger reduction in atmospheric growth rate (Figure 4, Figure S2).

245

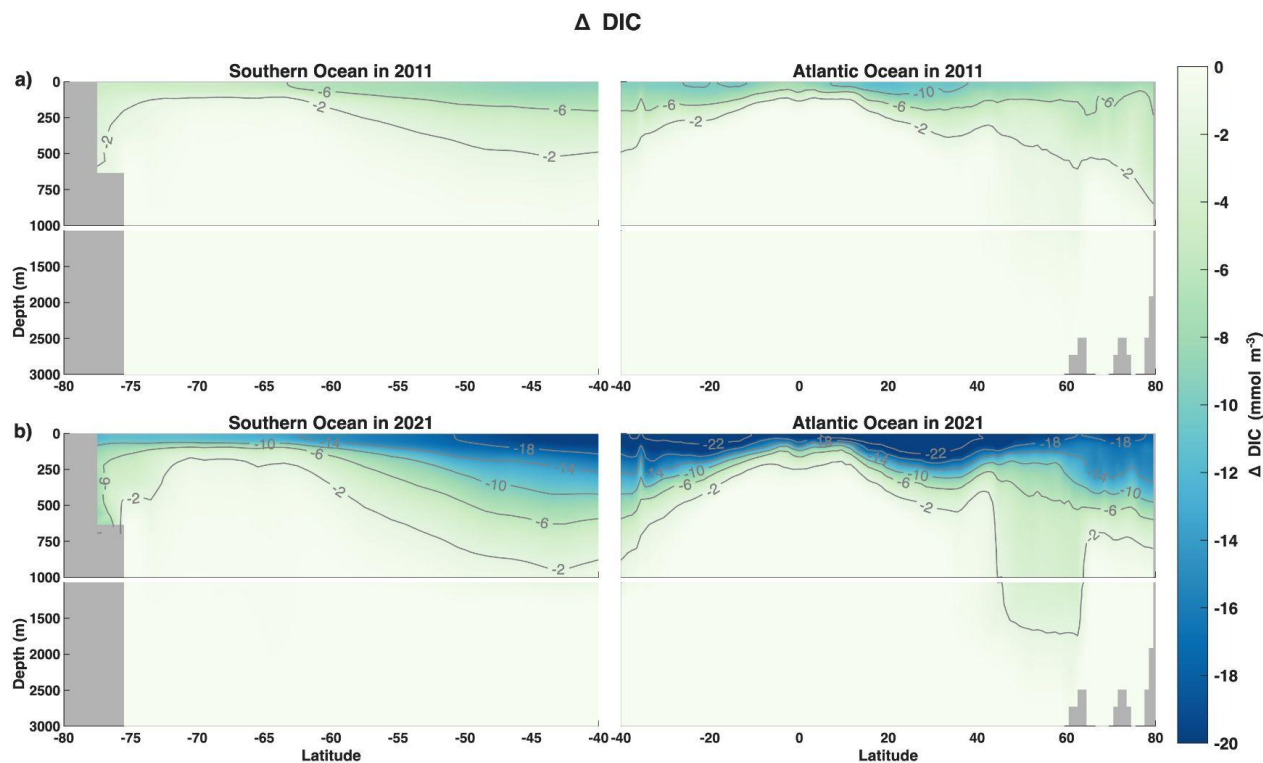


**Figure 4:** Southern Ocean and Atlantic basin-averaged zonal mean  $\Delta$ DIC concentration ( $\text{mmol m}^{-3}$ ) for SSP1 Mitigation minus Baseline. **a)** top panel shows changes in 2011 (11 years post mitigation), **b)** bottom panel shows 2021, (the last year of the simulation). Negative values (cooler colors) indicate more carbon accumulation in Baseline as compared to mitigation scenarios. Similar figure for results from SSP2 shown in Figure S2.

### 3.5 DIC Budget

In this section, we consider the three-dimensional tendency terms of DIC to better understand the ocean carbon cycle response to mitigation. We first present the Baseline and SSP1 total tendencies and then the SSP1–Baseline differences for the tendency and the advection and diffusion terms contributing to it.

The Baseline simulation shows a global upper-ocean DIC inventory that is generally increasing across most of the global oceans, reflecting the ongoing sequestration of anthropogenic carbon and its movement throughout the upper ocean (Figure 5a). Positive DIC tendencies (DIC gain) are prominent across the Southern Ocean and the Eastern Equatorial Pacific, driven by the vigorous upwelling of deep, DIC-rich waters and subsequent air-sea uptake in these regions. In contrast, the Western Equatorial Pacific exhibits a negative tendency (DIC loss), primarily due to the strong eastward transport of carbon via the Equatorial Undercurrent and horizontal advection away from the pool of accumulating surface carbon. In the Subpolar North



265

Atlantic, the tendency is near zero; while this is a region of intense uptake, the "missing" carbon is rapidly exported to the deep ocean through deep convection, preventing a large accumulation in the top 500 meters.

The SSP1 scenario exhibits a spatially similar pattern to the Baseline, but with a significant reduction in the magnitude of carbon gain (Figure 5b).

270

As shown in the  $\Delta$ DIC tendency (SSP1 minus Baseline) map (Figure 5c), the mitigation pathway results in a global declining signal, indicating that the rate of DIC accumulation is slower in SSP1 Mitigation than in the historical Baseline run. This difference is due only to the reduced atmospheric concentration, which weakens the air-sea gradient and subsequently alters the internal carbon budget through the mechanisms of advection and diffusion. The SSP1 mitigation scenario induces a rapid and widespread reduction in the DIC inventory tendency within the upper 500 meters compared to the Baseline run (Figure 5c). By the end of the simulation (2016–2021 time-mean), the  $\Delta$ DIC inventory tendency (SSP1 minus Baseline) peaks in the subtropical gyre regions, with regional differences reaching as low as  $-1.8 \times 10^{-5}$  Pg C year<sup>-1</sup> in the Southern hemisphere subtropics (Figure 5c). This negative tendency represents a significant slowdown in carbon accumulation under the aggressive mitigation pathway represented in SSP1.

275

280

The decomposition of the DIC budget into its dominant terms (Figure 5d–f), illustrates that air-sea flux is the primary driver of the global reduction in  $\Delta$ DIC. The change in the flux component is negative across the entire globe, indicating that the ocean takes up less carbon (or outgasses more) in the SSP1 scenario compared to the Baseline due to the lower atmospheric CO<sub>2</sub> concentration (Figure 1, 5f). While this flux impacts the DIC budget in the same direction across the globe, its magnitude varies spatially, with the strongest negative  $\Delta$ DIC values reaching ( $-2.6 \times 10^{-5}$  Pg C year<sup>-1</sup>) found in high-latitude regions.

285

290

While atmospheric mitigation dictates the global carbon inventory, changes in horizontal and vertical circulation determine the internal spatial reorganization of carbon in the upper-500 m. Net advection emerges as the primary redistributive mechanism, characterized by intense dipole patterns of both positive and negative  $\Delta$ DIC (Figure 5e). While the air-sea flux moves the DIC into the ocean, advection reorganizes where that carbon resides. This advective signal is dominated by horizontal transport across most of the globe (Figure 5g), particularly at current boundaries and within the Southern Ocean. Vertical advection plays a more localized but critical role, with prominent signals appearing in the Western Equatorial Pacific and at the convergence zones of major currents in the Southern Ocean (Figure 5h). Net diffusion is a minor contributor to the budget differences, appearing largely neutral (white) across most basins (Figure 5d).

295

Globally integrated over the 2016–2021 period, DIC tendency, circulation (net advection plus net diffusion), and air-sea CO<sub>2</sub> flux are  $-1.43$ ,  $0.132$ , and  $-1.56$  Pg C year<sup>-1</sup>, demonstrating that 1) DIC gain and loss from circulation largely compensates



when integrated globally and 2) the reduction in surface forcing (i.e., air-sea CO<sub>2</sub> flux) is the dominant driver of upper-ocean DIC variability when aggressive mitigation is applied.

300

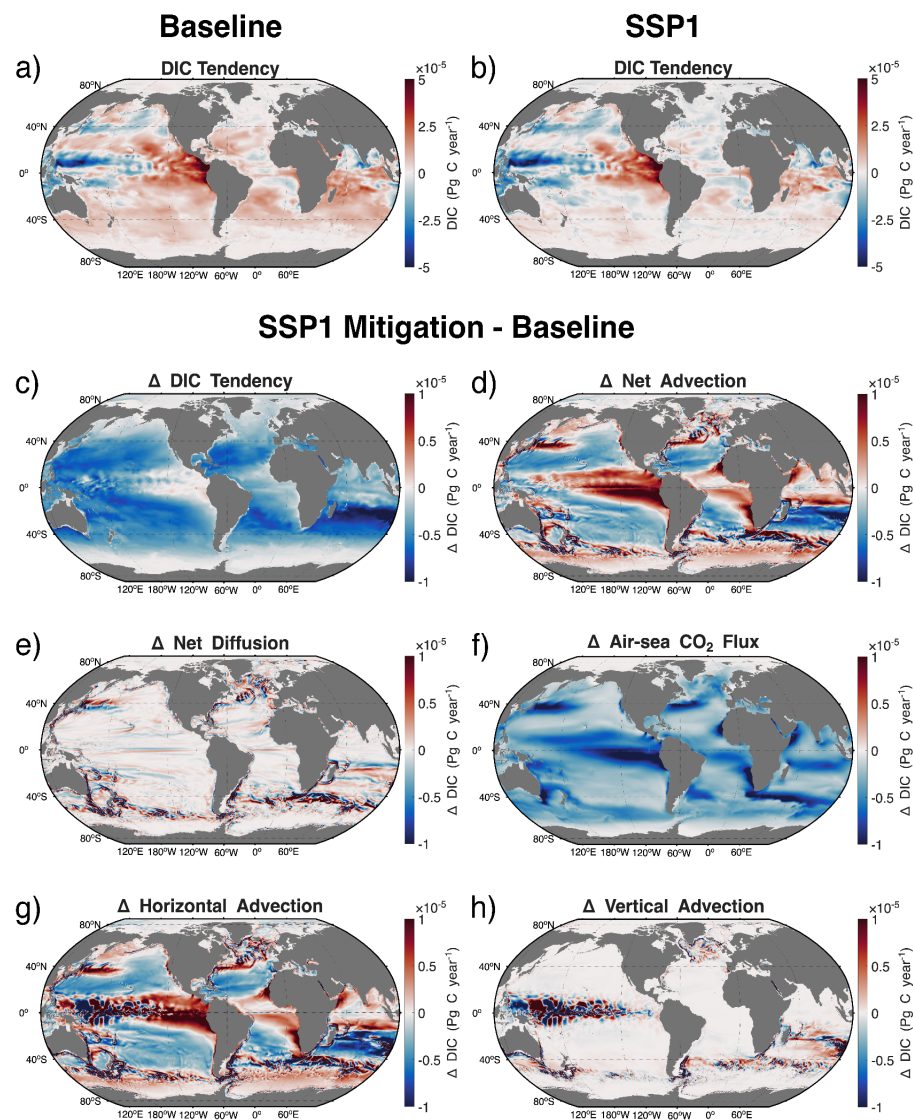


**Figure 5:** DIC budget. Time-mean (2016–2021) vertically integrated DIC tendency for (a) Baseline and (b) SSP1 Mitigation. Differences in ECCO-Darwin DIC budget terms (SSP1 Mitigation – Baseline) for surface-to-500 m vertically integrated 2016–2021 mean DIC tendency: (c) tendency, (d) net diffusion, (e) net advection, and (f) air-sea CO<sub>2</sub> flux. Net advection is further decomposed into (g) horizontal and (h) vertical components. A similar figure for SSP2 Mitigation is available in Figure S3.

305



### 3.6 Chemical Sensitivity: Revelle Factor and pH

To further understand the spatial heterogeneity of the mitigation-forced DIC differences, we examine the chemical capacity  
310 of the surface ocean to absorb carbon, quantified by the Revelle factor. The Revelle factor is a dimensionless ratio that  
describes the ocean's resistance to atmospheric CO<sub>2</sub> absorption. It is calculated as the fractional change in the partial pressure  
of carbon dioxide divided by the fractional change in total DIC. A higher Revelle factor indicates a lower buffering capacity  
and a higher sensitivity to changes. In the context of this study, the Revelle factor is a particularly critical diagnostic because  
the ECCO-Darwin model does not allow the sea-surface temperature (SST) fields to deviate between the Baseline and  
315 Mitigation simulations. Consequently, any observed differences in carbon uptake and storage between the scenarios are  
strictly isolated to changes in ocean circulation and the chemical buffering state, rather than thermal solubility effects.

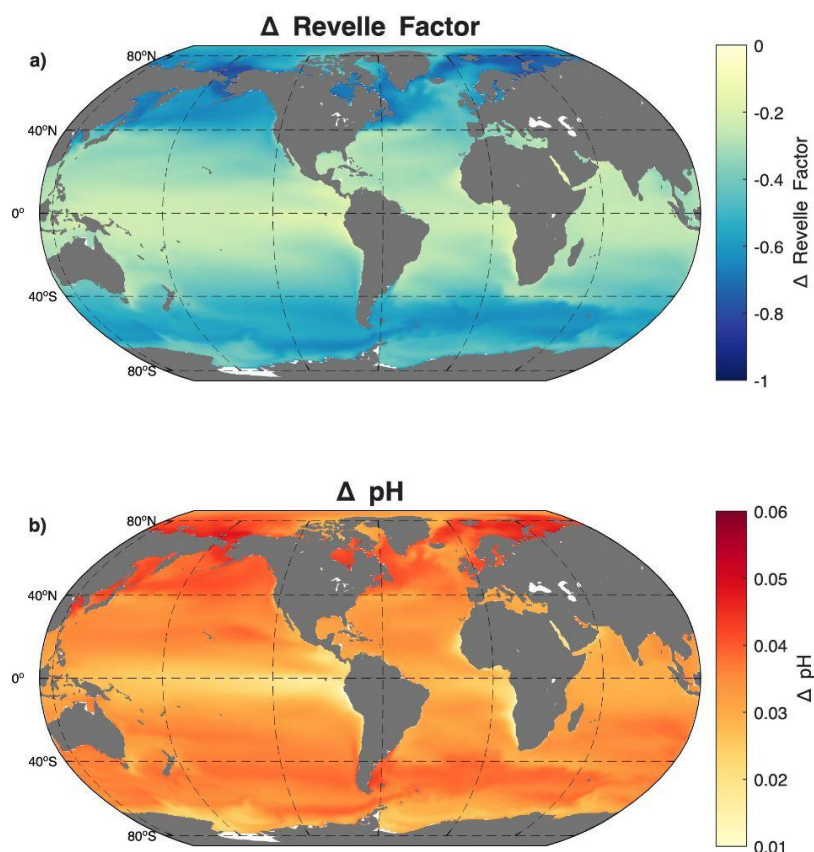
As shown in Figure 6a, the difference in Revelle factor (SSP1 minus Baseline) map reveals a global decline in the Revelle  
factor, signifying that the ocean surface becomes chemically "younger" and more receptive to carbon under mitigation than it  
320 would have been under sustained emissions. These changes are not uniform; while the subtropics remain relatively stable,  
the high latitudes — and most notably the Southern Ocean — exhibit the most significant reductions. This suggests that in  
these regions, the reduction in total DIC loading significantly enhances the chemical buffering potential. By isolating these  
chemical shifts from thermal feedback, something that is unique to the ECCO-Darwin model, a clearer attribution of the  
resulting DIC inventory changes can be attributed to the interplay between this renewed buffering capacity and the  
325 redistributive power of ocean circulation.

Complementing these buffering shifts, the difference in surface pH (Figure 6b) shows a global increase under the SSP1  
scenario relative to the Baseline. This positive anomaly indicates that the mitigation pathway effectively slows the  
progression of ocean acidification, with the Baseline ocean remaining significantly more acidic across all basins. Similar to  
330 the Revelle factor, the most pronounced pH recovery occurs in the high latitudes, where differences reach upwards of +0.05  
to +0.06 units. These polar regions, particularly the Southern Ocean, are highly sensitive to carbon loading due to their low  
background temperatures and naturally-higher DIC concentrations; thus, the reduction in DIC under SSP1 yields a  
disproportionately large mitigation benefit for pH. In contrast, the subtropics and equatorial regions exhibit more muted pH  
anomalies, reflecting their greater inherent chemical stability.

335 When viewed alongside the Revelle factor, the changes we see in pH values with mitigation highlight that the high latitudes  
are the primary beneficiaries of the chemical relief afforded by reduced atmospheric CO<sub>2</sub>. The spatial coherence between the  
Revelle factor and pH, along with the previously discussed DIC tendency maps, reveals a pronounced high latitude  
sensitivity. We stress that because these pH gains are achieved without the influence of temperature-driven solubility



340 changes, they represent a pure chemical response to the altered carbon inventory and the resulting shifts in the ocean's internal carbonate equilibrium.



345 **Figure 6:** Change in **a)** Revelle factor and **b)** pH (SSP1 Mitigation minus Baseline). Differences are time-averaged over 2016–2021. In a) negative  $\Delta$ Revelle factor values signify that the ocean surface is becoming chemically "younger" and more receptive to carbon under mitigation. In b) positive  $\Delta$ pH values indicate more acidic waters in the Baseline simulation.

#### 4. Discussion

350

##### 4.1 Global Ocean Carbon Sink Response to Mitigation



The global weakening of the ocean carbon sink under SSP1 and SSP2 Mitigation simulations, (corresponding to SSP1-1.9 and SSP1-2.6 scenarios, respectively) shown here as the rapid onset of divergence beginning in 2000, confirms previous findings that anthropogenic CO<sub>2</sub> emission mitigation immediately reduces oceanic uptake on annual to decadal timescales (Lovenduski et al. 2021). The prompt response of the air-sea flux (Figure 1) reflects the tight coupling between atmospheric pCO<sub>2</sub> and surface-ocean carbonate chemistry: reductions in atmospheric CO<sub>2</sub> diminish the air-sea gradient, reducing the flux into the ocean (McKinley et al. 2020).

The relationship between the magnitude of mitigation and the magnitude of the sink reduction is not strictly linear (Figure 1). This modest non-linearity likely reflects a combination of buffer chemistry, physical circulation, and biogeochemical feedbacks. For example, the interplay between the biological pump, changes in export production, and ecosystem shifts are simultaneously occurring along with the reduction in atmospheric CO<sub>2</sub> levels. Similar nonlinearity appears in CMIP6 Earth system models, where studies have documented a breakdown in the proportionality between atmospheric CO<sub>2</sub> and the ocean carbon sink under various mitigation scenarios (Terhaar, 2024, Gooya et al., 2023). Our results utilizing the ECCO-Darwin model for this experiment therefore align with the emerging understanding that emission mitigation will reduce the ocean carbon sink in some regions, but that internal climate system dynamics can strongly modulate the degree of change.

#### 4.2 Regional Sensitivity and Mechanisms

The spatial structure of mitigation-driven changes in cumulative air-sea CO<sub>2</sub> flux (Figure 3) highlights the dominant role of ocean circulation and ventilation in shaping the ocean carbon sink's response to reduced atmospheric forcing (Ridge and McKinley, 2021, Iudicone et al. 2016). The concentration of CO<sub>2</sub> flux reduction in the Southern and North Atlantic Oceans are consistent with their established role as primary gateways for anthropogenic carbon uptake (Gruber et al., 2019, 2023). These regions are well known to dominate global anthropogenic carbon uptake due to strong air-sea CO<sub>2</sub> exchange, deep mixed layers, and efficient ventilation and overturning circulation pathways that transport carbon from the surface to the ocean interior (Sabine et al., 2004; Khatiwala et al., 2009). In this experiment, the largest reductions in cumulative CO<sub>2</sub> uptake occur in the Southern and North Atlantic Oceans, identifying these regions as primary hotspots of mitigation sensitivity (Figure 3, 4). These regions are well known to dominate global anthropogenic carbon uptake due to strong air-sea CO<sub>2</sub> exchange, deep mixed layers, and efficient ventilation and overturning circulation pathways that transport carbon from the surface to the ocean interior (Sabine et al., 2004; Khatiwala et al., 2009; DeVries, 2014; Gruber et al., 2019; Lovenduski et al. 2021; Terhaar et al., 2022; Turner et al., 2023). The strong response in these regions is consistent with previous observational and modeling studies showing that changes in atmospheric CO<sub>2</sub> forcing are rapidly transmitted to the ocean interior where ventilation is efficient (Williams et al. 2023).



385 Western boundary current systems, including the Gulf Stream and Kuroshio Currents and their respective extensions exhibit pronounced reductions in uptake under both mitigation scenarios. These regions are characterized by intense mesoscale activity, strong vertical mixing, and rapid subduction of surface waters along isopycnals, which collectively enhance the communication between surface forcing and the thermocline (Cronin et al. 2010, Li et al. 2025). As a result, changes in atmospheric CO<sub>2</sub> forcing are efficiently communicated to the interior ocean in these regions, amplifying the local response of air-sea CO<sub>2</sub> flux. As shown by Carroll et al. (2022), in the ECCO-Darwin model, western boundary currents play a central role in regional DIC budgets by linking surface carbon uptake to interior storage pathways. In this sense, mitigation preferentially weakens carbon uptake where the physical system is most effective at exporting surface waters to depth (Williams et al. 2026, Li et al. 2022).

390

395 In contrast, much of the subtropical gyre interior exhibits comparatively weaker flux differences (Figure 3d,e). At the end of the simulation, the North Pacific STSS biome, which encompasses the Kuroshio region (Fay & McKinley 2014), the average reduction in air-sea CO<sub>2</sub> flux from Baseline to SSP1 Mitigation scenarios is 0.61 mol m<sup>-2</sup> yr<sup>-1</sup>, while in the nearby subtropical basin (NP STPS biome) the average reduction in flux is 0.26 mol m<sup>-2</sup> yr<sup>-1</sup>. A similar comparison exists in the North Atlantic regions as well. This suggests a slower or more muted response to mitigation on decadal timescales in the subtropical gyres.

400 These regions are characterized by shallower mixed layers, weaker vertical exchange, and longer ventilation timescales (Talley et al. 2011), which limit the rapid transmission of changes in atmospheric CO<sub>2</sub> to the ocean interior. This spatial contrast underscores the importance of ventilation timescales in governing where and when mitigation impacts emerge in the ocean carbon sink.

405 The spatial patterns identified here are broadly consistent with findings from CMIP5 and CMIP6 ESMs which consider mitigation scenarios. Broadly, previous multi-model analyses indicate that the Southern and North Atlantic Ocean dominate both present-day and future anthropogenic carbon uptake, but also exhibit the largest absolute changes in uptake under mitigation scenarios (McKinley et al. 2023, Katavouta & Williams 2021, Frölicher et al. 2015). Time-of-emergence studies using ESM output show that signals of changing carbon uptake appear earliest in these regions, while subtropical and tropical regions often exhibit delayed or masked responses due to internal variability and slower ventilation (McKinley et al. 2016, 2017, Schulenegger et al. 2020). These works show signals of changing ocean carbon uptake emerging in subpolar regions earliest, specifically within 10–30 years post mitigation. In contrast, subtropical and tropical regions display masked or delayed signals, often appearing after 50+ years, if at all, driven by higher internal variability and slower ventilation. Nevertheless, CMIP6 models also display substantial inter-model spread in the magnitude and spatial distribution of uptake changes, reflecting uncertainties in Southern Ocean mixing, boundary current and freshwater representation, and carbonate chemistry buffering (McKinley et al. 2023, Gooya et al. 2023, Katavouta & Williams 2021).

415



### 4.3 Ventilation and DIC Penetration

420 Zonal mean diagnostics provide a mechanistic view of how mitigation alters carbon penetration pathways over time, complementing the surface flux patterns shown earlier. In the North Atlantic Ocean, reductions in DIC accumulation under mitigation mirror regions of active ventilation (20–60°N), whereas in the Pacific and Indian basins (not shown), where thermocline ventilation is slower and deeper, there are weaker and more gradually emerging differences. The confinement of most mitigation DIC anomalies to the upper 500–1000 m is consistent with expected decadal ventilation timescales and  
425 indicates that deeper ocean sequestration is not strongly altered by short-term mitigation. Similar latitude-depth analyses have been used to diagnose ventilation and storage mechanisms in longer-term mitigation experiments (e.g., Ridge & McKinley, 2021), though the shorter simulation period considered here emphasizes early-stage adjustments rather than long-term equilibration.

430 Considering the drivers of  $\Delta$ DIC (SSP1 Mitigation minus Baseline) at the end of the simulation (2016–2021 mean), we find that net advection (horizontal plus vertical terms) and air-sea  $\text{CO}_2$  dominant the patterns of DIC gain and loss in the upper-500 m (Figure 5e,g,h). The DIC tendency term shows a large-scale reduction in DIC across most of the global ocean, with small DIC tendency values in the Arctic, Southern, and west Equatorial Pacific Oceans. This primarily results from DIC loss via a reduction in air-sea  $\text{CO}_2$  flux that is compensated by a gain of DIC from net advection. Net diffusion (Figure 5d,  
435 horizontal plus vertical terms) exhibits both gains and losses of DIC, which are primarily concentrated in boundary current regions where vertical mixing is substantial. As the ECCO-Darwin ecosystem is not carbon limited, changes in biological uptake between runs are negligible and not shown here.

### 4.4 Sensitivity to Chemical Changes

440 The global distributions of the  $\Delta$ Revelle Factor and  $\Delta$ pH (SSP1 minus Baseline) illustrate the immediate chemical relief provided by the mitigation pathway. Because the Revelle Factor is a measure of the ocean's resistance to absorbing  $\text{CO}_2$ , the predominantly negative anomalies, peaking at approximately  $-0.8$  to  $-1.0$  in the high latitudes, indicate that the Revelle factor is significantly higher in the Baseline run. This confirms that under sustained emissions, surface waters exhibit a lower buffering capacity and are chemically resistant to change, whereas the SSP1 scenario allows these waters to remain more  
445 receptive to ocean carbon absorption. Similarly, the  $\Delta$ pH map shows a global positive anomaly, meaning the Baseline ocean is more acidic than the SSP1 ocean. The magnitude of this difference is greatest in the high latitudes (reaching upwards of  $+0.05$ – $0.06$  pH units), a pattern that closely mirrors the Revelle factor anomalies and is consistent with a previous study assessing the pH response to emissions reductions (Lovenduski et al., 2021). The spatial coherence between these two chemical parameters and the previously discussed DIC tendency maps is striking, with significant high latitude sensitivity.

450

The largest changes in both pH and Revelle factor occur in the Southern Ocean and North Atlantic. These regions are naturally characterized by low temperatures and high background DIC, making their carbonate chemistry highly sensitive to



even small changes in total carbon loading. In the SSP1 scenario, the reduction in DIC (Figure 5c) slows the erosion of the buffering system that occurs in the Baseline, leading to a larger pH margin compared to the tropics. In contrast, the Equatorial Pacific shows a more muted change in pH (~0.02 units). While this region is a major site of CO<sub>2</sub> outgassing and DIC transport, its naturally lower Revelle factor (increased buffering) means that the difference in atmospheric CO<sub>2</sub> between the two scenarios does not shift the chemical equilibrium as drastically as it does in the cold, carbon-rich polar waters. The regions where pH remains the most unchanged under mitigation are the same regions where the air-sea CO<sub>2</sub> flux was the dominant driver of the DIC budget. This confirms that the atmospheric signal is being translated into a chemical signal most efficiently in the high latitudes, where the Revelle factor is most dynamic. This agrees with previous work that finds that cold waters have a lower ratio of Alkalinity to DIC, making them the "canaries in the coal mine" for mitigation impacts (Orr et al., 2005; Jiang et al., 2019).

Under the SSP1 mitigation pathway, the reduction in total DIC (Figure 5c) loading prevents this chemical saturation. The resulting lower Revelle factor (Figure 6a) indicates that for any given unit of atmospheric CO<sub>2</sub>, the Southern Ocean surface waters are more chemically receptive to carbon absorption. This means that, while the total magnitude of carbon uptake might be lower due to the reduced atmospheric gradient, the efficiency per unit of *p*CO<sub>2</sub> is significantly higher (Hauck et al., 2020). This chemical relationship is a critical feedback mechanism: by slowing the rise of the Revelle factor through mitigation, the ocean protects the solubility pump, which is essential to regulate the global carbon cycle in a lower-carbon future (Fassbender et al., 2017).

#### 4.5 Limitations

ECCO-Darwin's physical circulation fields are constrained to observations and reanalysis products and do not evolve dynamically under different climate states. Thus, our mitigation experiments do not capture feedbacks associated with warming-induced changes in stratification or wind stress that would occur in coupled climate models. Additionally, uncertainties in biological export and alkalinity cycling could influence the magnitude of DIC responses, though these are not considered in our analysis. Such changes would likely occur on the scale of 100 years. Despite these limitations, the ECCO-Darwin framework offers a unique strength: its physically-constrained circulation enables robust diagnosis of mechanistic responses, including ventilation pathways, regional recirculation, and upper-ocean storage of carbon.

The ECCO-based results presented here benefit from a physically-constrained circulation model that reproduces observed large-scale transport and ventilation pathways (Forget et al., 2015, Zhang et al., 2018, Carroll et al., 2020, 2022). This allows clear attribution of spatial patterns to specific mechanisms, such as boundary current subduction and high-latitude overturning. Our results isolate the direct response of the ocean carbon sink to atmospheric CO<sub>2</sub> mitigation without the confounding influence of climate-driven circulation and sea-ice changes that are present in CMIP6 projections.



## 5. Conclusions

Our ECCO-Darwin-based mitigation simulations show an immediate, but spatially heterogeneous weakening of the ocean carbon sink for anthropogenic carbon under reduced atmospheric CO<sub>2</sub> forcing. Global air-sea carbon uptake decreases substantially over the first several years of mitigation, with the magnitude scaling roughly with scenario strength. The bulk of the mitigation signal is confined to the upper 500 m, reflecting dominant decadal-scale ventilation pathways. The strongest reductions occur in subtropical thermocline regions, western boundary currents, and the subpolar North Atlantic Ocean. This is consistent with regions of intense ventilation and rapid air-sea equilibration. Mitigation-induced changes in ocean CO<sub>2</sub> uptake and storage are concentrated in regions that currently dominate anthropogenic carbon uptake and export to the interior (Sabine et al. 2004, Müller et al. 2023, Davila et al. 2022). This has important implications for both detection and projection of mitigation impacts. Observational efforts aimed at tracking changes in the ocean carbon sink are likely to be most effective in high-latitude ventilation regions and western boundary current systems, where signals are strongest and emerge earliest. Moreover, the strong sensitivity of these regions highlights their importance in determining how rapidly the ocean carbon sink adjusts to changes in anthropogenic forcing under future mitigation pathways.

In the context of a near-term and realistic physical ocean as portrayed by the ECCO-Darwin model, impacts of mitigation scenarios are as expected. Results align with complementary studies using CMIP models focused on longer-term responses (Ridge and McKinley 2021, Williams et al. 2023) to mitigation, short-term responses to COVID-like perturbations (Lovenduski et al. 2021), and ocean inversion estimates (Gruber et al. 2019, Khatiwala et al. 2009). The extent to which these projected changes would shape the observing system required to detect future change in the ocean carbon sink is a topic worthy of future study.

Overall, these results suggest that near-term mitigation produces an immediate and discernible weakening of ocean CO<sub>2</sub> uptake, particularly in regions of vigorous ventilation. This response has implications for carbon budget accounting and underscores the importance of sustained observations in tropical, subtropical, and high-latitude ventilation pathways to detect and attribute changes in air-sea CO<sub>2</sub> exchange under future climate mitigation strategies.

## Data Availability Statement

All ECCO-Darwin model output is available at the ECCO Data Portal: <http://data.nas.nasa.gov/ecco/>. Model code and platform-independent instructions for running the ECCO-Darwin simulations described in this study are available in Carroll et al. (2024a, 2024b).



### **Author contributions**

520 GAM, DC, DM, and ARF designed the experiments, and ARF, DC and HZ carried them out. HZ performed the simulations. ARF and DC led the analysis. ARF and DC prepared the manuscript with contributions from all co-authors.

### **Competing interests**

The authors declare that they have no conflict of interest.

### 525 **Financial Support**

AF and GAM acknowledge support from NASA Carbon Cycle Science via grant 80NSSC22K0150. DC and DM acknowledge support from the NASA Carbon Monitoring System. DC, DM, and HZ acknowledge support from the NASA Carbon Cycle Science program. NSL acknowledges support from the National Science Foundation (OCE-1752724).



## 530 References

- Carroll, D., Menemenlis, D., Adkins, J. F., Bowman, K. W., Brix, H., Dutkiewicz, S., et al. (2020). The ECCO-Darwin data-assimilative global ocean biogeochemistry model: Estimates of seasonal to multidecadal surface ocean pCO<sub>2</sub> and air-sea CO<sub>2</sub> flux. *Journal of Advances in Modeling Earth Systems*, 12(10), 1–28. <https://doi.org/10.1029/2019ms001888>
- Carroll, D., Menemenlis, D., Dutkiewicz, S., Lauderdale, J. M., Adkins, J. F., Bowman, K. W., et al. (2022). Attribution of  
535 space-time variability in global-ocean dissolved inorganic carbon. *Global Biogeochemical Cycles*, 36(3), e2021GB007162. <https://doi.org/10.1029/2021GB007162>
- Carroll, D., Menemenlis, D., Zhang, H., Mazloff, M., McKinley, G., Fay, A., et al. (2024a). *Evaluation of the ECCO-Darwin ocean biogeochemistry state estimate vs. in-situ observations* (ver 1.0) [Data set]. Zenodo. <https://doi.org/10.5281/zenodo.10627664>
- 540 Carroll, D., Zhang, H., Menemenlis, D., Bertin, C., Savelli, R., Manizza, M., et al. (2024b). *dustincarrolocean/ecco\_Darwin: v05 1985 back-extension* (1985\_back\_extension) [Software]. Zenodo. <https://doi.org/10.5281/zenodo.13259496>
- Carroll, D., Parazoo, N. C., Lovenduski, N. S., Keller, M., Schimel, D. S., & Bloom, A. A. (2025). Observing system needs for understanding carbon–climate feedbacks. *Environmental Research Letters*, 20(11), 111002. <https://doi.org/10.1088/1748-9326/ae0ae8>  
545 [9326/ae0ae8](https://doi.org/10.1088/1748-9326/ae0ae8)
- Cronin, M. F., Bond, N., Booth, J., Ichikawa, H., Joyce, T. M., Kelly, K., Kubota, M., Qiu, B., Reason, C., Rouault, M., & Sabine, C. (2010). Monitoring ocean-atmosphere interactions in western boundary current extensions. *Proceedings of OceanObs'09*. <https://doi.org/10.5270/OceanObs09.cwp.20>
- Davila, X., Gebbie, G., Brakstad, A., Lauvset, S. K., McDonagh, E. L., Schwinger, J., & Olsen, A. (2022). How is the ocean anthropogenic carbon reservoir filled? *Global Biogeochemical Cycles*, 36, e2021GB007055. <https://doi.org/10.1029/2021GB007055>  
550 <https://doi.org/10.1029/2021GB007055>
- DeVries, T. (2014). The oceanic anthropogenic CO<sub>2</sub> sink: Storage, air-sea fluxes, and transports over the industrial era. *Global Biogeochemical Cycles*, 28, 631–647. <https://doi.org/10.1002/2013GB004739>
- Fassbender, A. J., Sabine, C. L., & Palevsky, H. I. (2017). Nonuniform ocean acidification and attenuation of the ocean carbon sink. *Geophysical Research Letters*, 44(16), 8404–8413. <https://doi.org/10.1002/2017GL074389>  
555 <https://doi.org/10.1002/2017GL074389>



- Fay, A. R., & McKinley, G. A. (2014). Global open-ocean biomes: Mean and temporal variability. *Earth System Science Data*, 6, 273–284. <https://doi.org/10.5194/essd-6-273-2014>
- Fay, A. R., Carroll, D., McKinley, G. A., Menemenlis, D., & Zhang, H. (2024). Scale-dependent drivers of air-sea CO<sub>2</sub> flux variability. *Geophysical Research Letters*, 51, e2024GL111911. <https://doi.org/10.1029/2024GL111911>
- 560 Flato, G., Marotzke, J., Abiodun, B., Braconnot, P., Chou, S. C., Collins, W., Cox, P., Driouech, F., Emori, S., Eyring, V., Forest, C., Gleckler, P., Guilyardi, E., Jakob, C., Kattsov, V., Reason, C., & Rummukainen, M. (2013). Evaluation of climate models. In T. F. Stocker, D. Qin, G.-K. Plattner, M. Tignor, S. K. Allen, J. Boschung, A. Nauels, Y. Xia, V. Bex, & P. M. Midgley (Eds.), *Climate change 2013: The physical science basis. Contribution of Working Group I to the Fifth Assessment Report of the Intergovernmental Panel on Climate Change*. Cambridge University Press.
- 565 Follows, M. J., Dutkiewicz, S., Grant, S., & Chisholm, S. W. (2007). Emergent biogeography of microbial communities in a model ocean. *Science*, 315, 1843–1846. <https://doi.org/10.1126/science.1138544>
- Forget, G., Campin, J.-M., Heimbach, P., Hill, C., Ponte, R. M., & Wunsch, C. (2015). ECCO version 4: An integrated framework for non-linear inverse modeling and global ocean state estimation. *Geoscientific Model Development*, 8, 3071–3104. <https://doi.org/10.5194/gmd-8-3071-2015>
- 570 Friedlingstein, P., O'Sullivan, M., Jones, M. W., Andrew, R. M., Bakker, D. C., Hauck, J., et al. (2025). Global carbon budget 2025. *Earth System Science Data Discussions*, 1–139. <https://doi.org/10.5194/essd-18-3211-2026>
- Frölicher, T. L., Sarmiento, J. L., Paynter, D. J., Dunne, J. P., Krasting, J. P., & Winton, M. (2015). Dominance of the Southern Ocean in anthropogenic carbon and heat uptake in CMIP5 models. *Journal of Climate*, 28(2), 862–886. <https://doi.org/10.1175/JCLI-D-14-00117.1>
- 575 Gooya, P., Swart, N. C., & Hamme, R. C. (2023). Time-varying changes and uncertainties in the CMIP6 ocean carbon sink from global to local scale. *Earth System Dynamics*, 14(2), 383–398. <https://doi.org/10.5194/esd-14-383-2023>
- Gruber, N., Landschützer, P., & Lovenduski, N. S. (2019). The variable Southern Ocean carbon sink. *Annual Review of Marine Science*, 11(1), 159–186. <https://doi.org/10.1146/annurev-marine-121916-063407>
- 580 Gruber, N., Bakker, D. C., DeVries, T., Gregor, L., Hauck, J., Landschützer, P., et al. (2023). Trends and variability in the ocean carbon sink. *Nature Reviews Earth & Environment*, 4(2), 119–134. <https://doi.org/10.1038/s43017-022-00381-x>



- Hauck, J., Zeising, M., Le Quéré, C., Gruber, N., Bakker, D. C., Bopp, L., Chau, T. T. T., Gürses, Ö., Ilyina, T., Landschützer, P., & Lenton, A. (2020). Consistency and challenges in the ocean carbon sink estimate for the global carbon budget. *Frontiers in Marine Science*, 7, 571720. <https://doi.org/10.3389/fmars.2020.571720>
- 585 Jiang, L.-Q., Carter, B. R., Feely, R. A., Lauvset, S. K., & Olsen, A. (2019). Surface ocean pH and buffer capacity: Past, present and future. *Scientific Reports*, 9(1), 18624. <https://doi.org/10.1038/s41598-019-55039-4>
- Katavouta, A., & Williams, R. G. (2021). Ocean carbon cycle feedbacks in CMIP6 models: Contributions from different basins. *Biogeosciences*, 18(10), 3189–3218. <https://doi.org/10.5194/bg-18-3189-2021>
- Khatiwala, S., Primeau, F., & Hall, T. (2009). Reconstruction of the history of anthropogenic CO<sub>2</sub> concentrations in the ocean. *Nature*, 462, 346–349. <https://doi.org/10.1038/nature08526>
- 590 Lan, X., Tans, P., Thoning, K., & NOAA Global Monitoring Laboratory. (2024). NOAA Greenhouse Gas Marine Boundary Layer Reference - CO<sub>2</sub>. [Data set]. NOAA GML. <https://doi.org/10.15138/DVNP-F961>
- Lee, H., Noh, K. M., Oh, J. H., Park, S. W., Shin, Y., & Kug, J. S. (2025). Emergence of an oceanic CO<sub>2</sub> uptake hole under global warming. *Nature Communications*, 16(1), 3199. <https://doi.org/10.1038/s41467-025-57724-7>
- Li, C., Zhai, W., & Qi, D. (2022). Unveiling controls of the latitudinal gradient of surface pCO<sub>2</sub> in the Kuroshio Extension and its recirculation regions (northwestern North Pacific) in late spring. *Acta Oceanologica Sinica*, 41(5), 110–123. <https://doi.org/10.1007/s13131-021-1949-1>
- 595 Li, X., Gan, B., Zhang, Z., Cao, Z., Qiu, B., Chen, Z., & Wu, L. (2025). Oceanic uptake of CO<sub>2</sub> enhanced by mesoscale eddies. *Science Advances*, 11(24), eadt4195. <https://doi.org/10.1126/sciadv.adt4195>
- Meinshausen, M., Nicholls, Z. R. J., Lewis, J., Gidden, M. J., Vogel, E., Freund, M., Beyerle, U., Gessner, C., Nauels, A., 600 Bauer, N., Canadell, J. G., Daniel, J. S., John, A., Krummel, P. B., Luderer, G., Meinshausen, N., Montzka, S. A., Rayner, P. J., Reimann, S., Smith, S. J., van den Berg, M., Velders, G. J. M., Vollmer, M. K., & Wang, R. H. J. (2020). The shared socio-economic pathway (SSP) greenhouse gas concentrations and their extensions to 2500. *Geoscientific Model Development*, 13, 3571–3605. <https://doi.org/10.5194/gmd-13-3571-2020>
- 605 Müller, J. D., Gruber, N., Carter, B., Feely, R., Ishii, M., Lange, N., et al. (2023). Decadal trends in the oceanic storage of anthropogenic carbon from 1994 to 2014. *AGU Advances*, 4, e2023AV000875. <https://doi.org/10.1029/2023AV000875>



- O'Neill, B. C., Tebaldi, C., van Vuuren, D. P., Eyring, V., Friedlingstein, P., Hurtt, G., Knutti, R., Kriegler, E., Lamarque, J.-F., Lowe, J., Meehl, G. A., Moss, R., Riahi, K., & Sanderson, B. M. (2016). The Scenario Model Intercomparison Project (ScenarioMIP) for CMIP6. *Geoscientific Model Development*, 9, 3461–3482. <https://doi.org/10.5194/gmd-9-3461-2016>
- 610 Orr, J. C., Fabry, V. J., Aumont, O., Bopp, L., Doney, S. C., Feely, R. A., Gnanadesikan, A., Gruber, N., Ishida, A., Joos, F., & Key, R. M. (2005). Anthropogenic ocean acidification over the twenty-first century and its impact on calcifying organisms. *Nature*, 437(7059), 681–686. <https://doi.org/10.1038/nature04095>
- Riahi, K., van Vuuren, D. P., Kriegler, E., Edmonds, J., O'Neill, B. C., Fujimori, S., et al. (2017). The Shared Socioeconomic Pathways and their energy, land use, and greenhouse gas emissions implications: An overview. *Global Environmental Change*, 42, 153–168. <https://doi.org/10.1016/j.gloenvcha.2016.05.009>
- 615 Ridge, S. M., & McKinley, G. A. (2021). Ocean carbon uptake under aggressive emission mitigation. *Biogeosciences*, 18, 2711–2725. <https://doi.org/10.5194/bg-18-2711-2021>
- Sabine, C. L., Feely, R. A., Gruber, N., Key, R. M., Lee, K., Bullister, J. L., Wanninkhof, R., Wong, C. S. L., Wallace, D. W., Tilbrook, B., & Millero, F. J. (2004). The oceanic sink for anthropogenic CO<sub>2</sub>. *Science*, 305(5682), 367–371. <https://doi.org/10.1126/science.1097403>
- 620 Schimel, D. S., & Carroll, D. (2024). Carbon cycle–climate feedbacks in the post-Paris world. *Annual Review of Earth and Planetary Sciences*, 52(1), 467–493. <https://doi.org/10.1146/annurev-earth-031621-081700>
- Talley, L. D. (2011). *Descriptive physical oceanography: An introduction*. Academic Press.
- Terhaar, J., Frölicher, T. L., & Joos, F. (2021). Southern Ocean anthropogenic carbon sink constrained by sea surface salinity. *Science Advances*, 7(18), eabd5964. <https://doi.org/10.1126/sciadv.abd5964>
- 625 Terhaar, J., Frölicher, T. L., & Joos, F. (2022). Observation-constrained estimates of the global ocean carbon sink from Earth system models. *Biogeosciences*, 19(18), 4431–4457. <https://doi.org/10.5194/bg-19-4431-2022>
- Terhaar, J. (2024). Drivers of decadal trends in the ocean carbon sink in the past, present, and future in Earth system models. *Biogeosciences*, 21(17), 3903–3926. <https://doi.org/10.5194/bg-21-3903-2024>
- 630 Turner, K. E., Smith, D. M., Katavouta, A., & Williams, R. G. (2023). Reconstructing ocean carbon storage with CMIP6 Earth system models and synthetic Argo observations. *Biogeosciences*, 20, 1671–1690. <https://doi.org/10.5194/bg-20-1671-2023>



Williams, R. G., Meijers, A. J., Roussenov, V. M., Katavouta, A., Ceppi, P., Rosser, J. P., & Salvi, P. (2024). Asymmetries in the Southern Ocean contribution to global heat and carbon uptake. *Nature Climate Change*, 14(8), 823–831.

<https://doi.org/10.1038/s41558-024-02066-3>

635 Williams, R. G., Brown, P. J., Takano, Y., Forget, G., Jones, D., Katavouta, A., McDonagh, E., & Roussenov, V. M. (2026). The biogeochemical transport by the Gulf Stream. *Communications Earth & Environment*, 7(1), 149.

<https://doi.org/10.1038/s43247-025-03118-y>

Zhang, H., Menemenlis, D., & Fenty, I. (2018). *ECCO LLC270 ocean-ice state estimate*. MIT DSpace.

<https://dspace.mit.edu/handle/1721.1/119821>

640

645

650